

Design and Performance Analysis of a New STBC-MIMO LoRa System

Huan Ma, Guofa Cai, Yi Fang, Pingping Chen, Guojun Han

Abstract—LoRa is a modulation technology for low power wide area networks (LPWAN) with enormous potential in 5G era. However, the performance of LoRa system deteriorates seriously in fading-channel environments. To tackle this problem, in this paper we introduce multiple-input-multiple-output (MIMO) configuration employing space-time block coding (STBC) schemes into the LoRa system to formulate an STBC-MIMO LoRa system. Then, we investigate the theoretical performance of the proposed system over Rayleigh fading channels. To this end, we derive the distribution of the decision metric for the demodulator in the proposed system. Based on the above distribution, we propose the closed-form approximated bit error rate (BER) expression of the proposed system when perfect and imperfect channel information states (CSIs) are considered. In addition, we analyze the diversity order of the proposed system. The result demonstrates that the diversity order of the system in the imperfect CSI scenario with fixed channel estimate error variance is zero. However, in the imperfect CSI scenario with a decreasing channel estimate error variance and the perfect CSI scenario, the system can achieve full diversity. Finally, experimental results verify the accuracy of the theoretical analysis and the excellent performance of the proposed system. Due to such superiority, the proposed STBC-MIMO LoRa system can be considered as a good scheme for LPWAN.

Index Terms—Internet of things (IoT), LoRa, bit error rate (BER), space-time block coding (STBC), multiple-input-multiple-output (MIMO), diversity order, Rayleigh fading channel.

I. INTRODUCTION

With the continuous update and improvement of Internet of things (IoT) and 5G technologies, massive connectivity has become one of the most important backbone of current world development. By providing real-time information, analysis and decision-making, the IoT in the 5G era is greatly changing the previous business models and lifestyles of people, such as driverless cars, unmanned aerial vehicle, smart appliances, and automated factories, thereby bringing unlimited possibilities for the future development of society. The widely promoted low power wide area network (LPWAN) plays an important role in 5G networks in recent years [1], because it can complement traditional cellular and short-range wireless technologies to address the different requirements of IoT applications. It is estimated that in 2022, the number of compatible nodes for LPWAN will reach 350 million [2].

For LPWAN, several communication technologies have been proposed, such as NB-IoT [3], Sigfox [4], and LoRa

[5], [6]. Compared with NB-IoT- and Sigfox-based LPWAN, LoRa-based LPWAN has some unique advantages such as highly open and flexible. Furthermore, LoRa-based LPWAN can be deployed in a private network and the operating cost of this LPWAN is low. As a modulation scheme of LPWAN, LoRa has gained considerable commercial traction and its specifications are maintained by the LoRa Alliance.¹ LoRa is a low-power, low-speed, and long-range modulation based on chirp spread-spectrum (CSS) technology [7]. In the LoRa modulation, cyclic shifts of chirp signal with linearly increased frequency form a multidimensional space for LoRa symbols, and the signals of different LoRa symbols are orthogonal to each other [8]. The coverage of LoRa is determined by the spreading factor. Increasing the spreading factor can provide wider coverage but reduce the data rate [9].

With the expansion of the market share occupied by LoRa in LPWAN, the number of countries deploying LoRa-based solutions has grown rapidly, which has reached 142 [6]. Accordingly, LoRa has also attracted more and more attention from academia. To explore various performance indicators of the LoRa modulation, researchers have carried out a lot of experimental-based works in the real world. In [10]–[13], the coverage capability of LoRa has been studied. In different scenarios, the coverage of LoRa ranges from 100m to 30km. In [12], the coverage of LoRa in outdoor scenario has been evaluated by deploying LoRa base station on a mountain. The results of the study indicate that the LoRa base station at an altitude of 470m can cover an area of 1380 square kilometers. In [13], it has been observed that the available communication distances of LoRa are 15km in the ground environment and 30km in the water environment.

After some pioneering work based on experiments, research on LoRa networks has attracted growing interest. With the increasing density of IoT applications, some work has considered the scalability and capacity of LoRa. In [14], the mathematical tools has been utilized to simulate the uplink coverage of the single gateway LoRa network and it reveals the unique physical layer characteristics of the LoRa network. In [15], scalability performance has been conducted on a LoRa network with multiple gateways, and the impact of confirmed and unconfirmed messages on the traffic of a large-scale LoRa network has been analyzed. In addition, theoretical LoRa capacity has been explored in [16]–[18], where ALOHA network model is utilized to characterize LoRa-based LPWAN. In [19], a more practical model considering capture effect has been adopted to analyze LoRa capacity. Moreover, some

H. Ma, G. Cai, Y. Fang and G. Han are with the School of Information Engineering, Guangdong University of Technology, Guangzhou 510006, China (e-mail: mh-zs@163.com; caiguofa2006@126.com; fangyi@gdut.edu.cn; gjhan@gdut.edu.cn).

P. Chen is with the Department of Electronic Information, Fuzhou University, Fuzhou 350116, China (e-mail: pphen.xm@gmail.com).

¹<https://lora-alliance.org>

recent research works have been studied to design multi-hop and multi-relay schemes for improving reliability of LoRa networks, e.g., concurrent transmission multi-hop LoRa network [20], multi-hop LoRa network with tree-based spreading factor clustering algorithm [21], and cooperative LoRa networks [22], [23].

While the LoRa physical layer is protected by patent [24], the study on such a modulation has become more active recently due to the implementation of reverse engineering [25], [26]. A rigorous mathematical description of the LoRa modulation and demodulation process has been developed in [8], and subsequently the waveform and spectral characteristics of the LoRa modulation have been investigated in [27]. In addition, bit-error-rate (BER) performance analysis of the LoRa modulation has been performed in [28], [29]. The analytical results show that the poor performance of the LoRa system might not sustain long-range communication in the fading environment. For this reason, some improved modulation schemes based on the physical layer of LoRa have been proposed, such as phase-shift-keying (PSK) LoRa [30], interleaved chirp spreading LoRa [31], and dual orthogonal LoRa [32]. All of these schemes aim at enhancing the capacity of the LoRa network. A LoRa-aided binary PSK multiple-input multiple-output (MIMO) system has been presented in [33]. The MIMO LoRa system can achieve better BER performance compared with the single-input single-output (SISO) LoRa system. However, the LoRa symbol in this system is only utilized to spread the spectrum of the BPSK baseband signal rather than carrying information, which leads to severe data-rate loss.

With the above motivation and considerable scalability of LoRa [6], this paper propose a space-time block-coded (STBC) MIMO scheme [33]–[36] with the LoRa modulation. The contributions of this paper are summarized as follows:

- 1) An STBC-MIMO LoRa system with M transmit antennas and N receive antennas is put forward. The proposed system can greatly improve BER performance, thereby enhancing the reliability of LoRa networks in fading-channel environments.
- 2) The theoretical BER performance of the proposed system is carefully analyzed over Rayleigh fading channels. Based on the principle of the STBC-MIMO scheme, the theoretical model of the proposed system is established, then the distribution of the decision metric for the demodulator of the proposed system is derived. According to the above distribution, the closed-form approximated BER expression of the proposed system is presented for both perfect and imperfect channel information states (CSIs). In particular, two common channel estimation error models (CEEMs) are considered in the analysis.
- 3) The asymptotic BER performance is investigated to analyze the diversity order of the proposed system. The results indicate indicates that for the fixed channel estimation error variance, the system reaches zero diversity order, while for the perfect CSI and channel estimation error variance being a decreasing function of average signal-to-noise ratio (SNR), the system can achieve full diversity $d = MN$.

- 4) Simulation results not only demonstrate the superior performance of the proposed STBC-MIMO LoRa system, but also verify the accuracy of the approximated BER expressions and diversity-order analysis.

The remainder of the paper is organized as follows. In Section II, we provide the detailed descriptions of the LoRa modulation/demodulation process and the proposed STBC-MIMO LoRa system. In Section III, we present the closed-form approximated BER expressions of the proposed system for perfect and imperfect CSIs. We also analyze the diversity order of the proposed system in the same Section. In Section IV, we present various simulation results with some discussions. Finally, Section V concludes the paper.

II. SYSTEM MODEL

A. LoRa Modulation

LoRa is a frequency shift CSS based modulation scheme. In the LoRa modulation, the frequency of the baseband signal varies linearly in a symbol duration and the bandwidth of the LoRa signal is B_w . There are 2^{SF} chips in each LoRa symbol, where $SF \in \{7, 8, \dots, 12\}$ is the spreading factor of LoRa. For a LoRa symbol x_o , it can carry SF bits, and assuming that the o^{th} transmitted symbol is $s_o = p \in \{0, 1, \dots, 2^{SF-1}\}$. The frequency of x_o varies linearly from the starting frequency $f_s = \frac{B_w \cdot p}{2^{SF}}$ to B_w and then folds to 0, in the remaining symbol duration, the frequency continues to change linearly from 0 to f_s [18]. Specifically, the frequency of each chip increases by $\frac{B_w}{2^{SF}}$. Therefore, the discrete-time baseband signal of the LoRa symbol x_o can be expressed as [18]

$$\begin{aligned} w_o(\kappa T_c) &= \sqrt{E_s} \bar{w}_p(\kappa T_c) \\ &= \sqrt{\frac{E_s}{2^{SF}}} \exp \left[j2\pi \left(\frac{((p + \kappa) \bmod 2^{SF})^2}{2^{SF+1}} \right) \right], \end{aligned} \quad (1)$$

where $T_c = \frac{1}{B_w}$ is the sample interval, κ denotes the index of the sample at time κT_c , E_s is the symbol energy, and $\bar{w}_p(\kappa T_c)$ is the basis function of $w_o(\kappa T_c)$. As seen from Eq. (1), the LoRa signal transmitting the symbol p can be considered as a cyclic shift of pT_c for the basis CSS signal [18], [28].² Since chirp signals with different offsets are mutually orthogonal, for the LoRa signal of the symbol s_o , when it correlates with 2^{SF} possible LoRa signals, it has the following properties [28]

$$\Lambda_i = \sum_{\kappa=0}^{2^{SF}-1} w_o(\kappa T_c) \cdot \bar{w}_i^*(\kappa T_c) = \begin{cases} \sqrt{E_s}, & i = p \\ 0, & i \neq p \end{cases}, \quad (2)$$

where $0 \leq i \leq 2^{SF} - 1$ and $*$ is the complex conjugate operation. The demodulation of the LoRa signal can be performed based on the above properties. For a received signal $r_o(\kappa T_c)$ of the LoRa symbol x_o after transmission over a frequency-flat

²The basic CSS signal can also be called as the *upchirp* signal, and its frequency varies linearly from 0 to B_w in a symbol duration.

and time-invariant channel, the output of the correlator in the LoRa demodulator is written as [28]

$$\begin{aligned} \hat{\Lambda}_i &= \sum_{\kappa=0}^{2^{SF}-1} r_o(\kappa T_c) \cdot \bar{w}_i^*(\kappa T_c) \\ &= \sum_{\kappa=0}^{2^{SF}-1} \left(\sqrt{h_c} w_o(\kappa T_c) + w_n(\kappa T_c) \right) \cdot \bar{w}_i^*(\kappa T_c) \\ &= \begin{cases} \sqrt{h_c E_s} + w_{n,i}, & i = p \\ w_{n,i}, & i \neq p \end{cases}, \end{aligned} \quad (3)$$

where $\sqrt{h_c}$ is the complex envelope amplitude, $w_n(\kappa T_c)$ is the complex additive Gaussian white noise (AWGN), and $w_{n,i}$ is the corresponding complex Gaussian noise process [31]. Hence, the symbol s_o can be estimated as

$$\hat{s}_o = \arg \max_{i=0, \dots, 2^{SF}-1} \left(|\hat{\Lambda}_i| \right), \quad (4)$$

where $|\cdot|$ denotes absolute operation. In addition, another equivalent low complexity method can also be utilized for demodulation. First, the received signal is multiplied with downchirp $\bar{w}_{down}(\kappa T_c)$ (this step is called a *dechirping*) [18], where $\bar{w}_{down}(\kappa T_c)$ can be expressed as

$$\bar{w}_{down}(\kappa T_c) = \sqrt{\frac{1}{2^{SF}}} \exp \left(-j2\pi \frac{\kappa^2}{2^{SF+1}} \right). \quad (5)$$

Afterwards, the 2^{SF} -point discrete Fourier transform (DFT) is performed on the dechirped signal, thus one can obtain as

$$\hat{\Lambda}_F = \text{DFT}(\mathbf{r}_o \odot \bar{\mathbf{w}}_{down}), \quad (6)$$

where $\hat{\Lambda}_F = [\hat{\Lambda}_{F,0}, \dots, \hat{\Lambda}_{F,i}, \dots, \hat{\Lambda}_{F,2^{SF}-1}]$, $\mathbf{r}_o = [r_o(0), r_o(T_c), \dots, r_o((2^{SF}-1)T_c)]$, $\bar{\mathbf{w}}_{down} = [\bar{w}_{down}(0), \bar{w}_{down}(T_c), \dots, \bar{w}_{down}((2^{SF}-1)T_c)]$, and \odot is the Hadamard product operator [37]. Next, the LoRa symbol is estimated by selecting the index of the frequency bin with the maximum magnitude, given by

$$\hat{s}_o = \arg \max_{i=0, \dots, 2^{SF}-1} \left(|\hat{\Lambda}_{F,i}| \right). \quad (7)$$

B. The Proposed STBC-MIMO LoRa System

In this paper, we consider a wireless MIMO system with M transmit antennas and N receive antennas that operates over a flat and quasi-static Rayleigh fading channel, therefore the path gains remain constant in a frame of J symbols and varies from a frame to another. We represent the MIMO channel as an $M \times N$ matrix, $\mathbf{H} = \{h_{m,n}\}$, where $h_{m,n}$ denotes the complex channel gain from the m^{th} transmit antenna to the n^{th} receive antenna. $h_{m,n}$ are independent random variables that follow complex Gaussian distribution with zero mean and variance 0.5 per dimension. Fig. 1 illustrates one possible realization on the transmitter and receiver of the proposed STBC-MIMO LoRa system, it is worth noting that the channel estimation module is in the STBC decoder

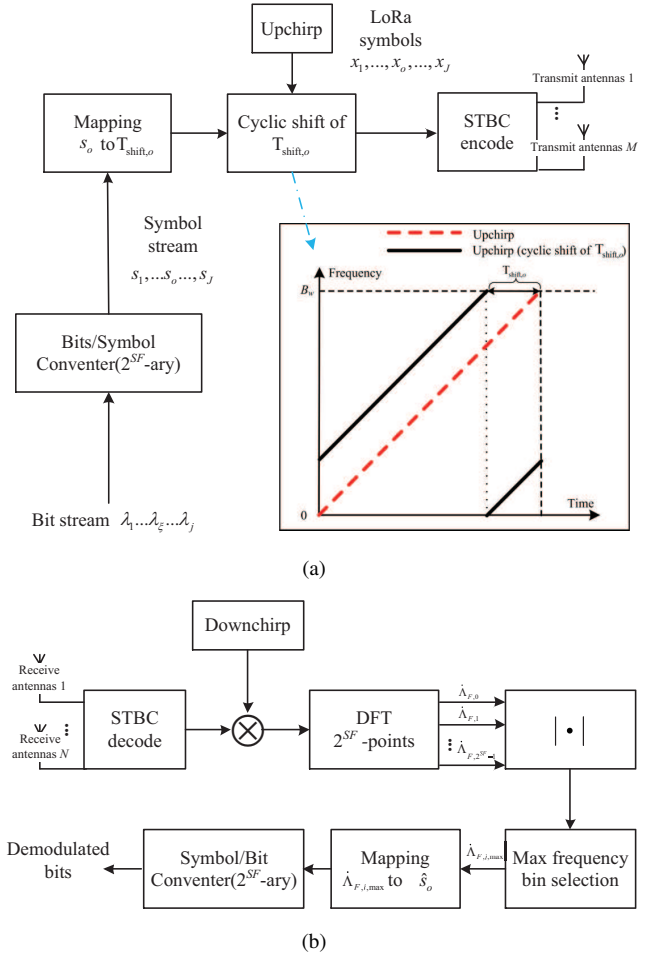


Fig. 1. Illustration of one possible realization of (a) transmitter and (b) receiver for the proposed STBC-MIMO LoRa system.

structure.³ A complex orthogonal STBC transmission matrix \mathbf{G} is represented by a $U \times M$ transmission matrix, where the entries are linear combinations of g_1, g_2, \dots, g_J and their conjugates. Moreover, matrix \mathbf{G} satisfies complex orthogonality $\mathbf{G}^H \mathbf{G} = u_{cons} (|g_1|^2 + \dots + |g_J|^2) \mathbf{I}_M$ [40], [41], where \mathbf{I}_M is an $M \times M$ identity matrix and u_{cons} is a constant that depends on the STBC transmission matrix [42]. Matrix \mathbf{G} is utilized to encode J ($J \geq 2$) input symbols into an M -dimensional vector sequence of U time slot (i.e., to control the symbol transmission of M transmitting antennas in each slot). Consequently, the transmission rate of STBC is $r = J/U$.

In this paper, the channel estimation matrix at the receiver is modeled as [43]–[45]

$$\hat{\mathbf{H}} = \mathbf{H} + \mathbf{E}_h, \quad (8)$$

where $\mathbf{E}_h = \{e_{m,n}\}$ is an $M \times N$ error matrix independent of \mathbf{H} , $e_{m,n}$ are complex Gaussian independent random variables with zero mean and variance σ_e^2 , where σ_e^2 reflects the accuracy of the channel estimation. Accordingly, the variance of the estimated channel gain is $\sigma_h^2 = \sigma_h^2 + \sigma_e^2$. In particular,

³Since the LoRa system can be regarded as a chirp-modulated high-order 2^{SF} -ary FSK system, the proposed STBC-MIMO LoRa system can adopt the pilot-based channel estimation method which is applicable to the FSK system [38], [39].

TABLE I
THE ENCODING AND TRANSMISSION SEQUENCE FOR THE PROPOSED
STBC-MIMO LoRa SYSTEM WITH TWO TRANSMIT ANTENNAS

	Transmit antenna 1	Transmit antenna 2
Time t_s	x_1	x_2
Time $t_s + 2^{SF}T_c$	$-x_2^*$	x_1^*

TABLE II
THE NOTATION FOR THE RECEIVED SIGNAL AT THE TWO RECEIVE
ANTENNAS

	Receive antenna 1	Receive antenna 2
Time t_s	r_1	r_3
Time $t_s + 2^{SF}T_c$	r_2	r_4

when $\sigma_e^2 = 0$, it can be considered that perfect channel estimation is performed at the receiver (i.e., the receiver knows perfect CSI). In this paper, two types of channel estimation error variance are considered: one is that σ_e^2 is fixed and independent of the average SNR, and the other is that σ_e^2 is a decreasing function of the average SNR. These two types of error variance correspond to CEEMs I and II, respectively. For the proposed STBC-MIMO LoRa system, when the channel estimation error occurs at the receiver, it causes inter-antenna interference (IAI). Here, we take the STBC \mathbf{G}_2 in [46] as an example and apply it to an STBC-MIMO LoRa system with two receive antennas to illustrate the encoding/decoding process in the proposed system. Code \mathbf{G}_2 is given by

$$\mathbf{G}_2 = \begin{pmatrix} g_1 & g_2 \\ -g_2^* & g_1^* \end{pmatrix}. \quad (9)$$

Utilizing \mathbf{G}_2 , we can encode the LoRa symbol in space and time. Taking the encoding of the first two LoRa symbols x_1 (the symbol transmitted by x_1 is $s_1 = p$) and x_2 (the symbol transmitted by x_2 is $s_2 \neq p$) in the sequence as an example, this process is shown in Table I. Correspondingly, the notation for the received signal at the two receive antennas is defined in Table II, where

$$\begin{aligned} r_1 &= h_{1,1}x_1 + h_{2,1}x_2 + n_1 \\ r_2 &= -h_{1,1}x_2^* + h_{2,1}x_1^* + n_2 \\ r_3 &= h_{1,2}x_1 + h_{2,2}x_2 + n_3 \\ r_4 &= -h_{1,2}x_2^* + h_{2,2}x_1^* + n_4, \end{aligned} \quad (10)$$

and n_1, n_2, n_3 , and n_4 are the complex AWGN with variance $N_0/2$ per dimension. Next, the maximum likelihood decoding of the STBC can be achieved by linear processing [46] in the STBC decoder at the receiver, thereby recovering the desired LoRa symbols. Without loss of generality, we take x_1 as an example for illustration and following analysis. For the LoRa symbol x_1 , LoRa symbols that carrying other transmitted symbols (i.e., the symbol is not equal to p) can be regarded as interference. After STBC decoding, the recovered LoRa

symbol \tilde{x}_1 can be expressed as

$$\begin{aligned} \tilde{x}_1 &= \hat{h}_{1,1}^* r_1 + \hat{h}_{2,1} r_2^* + \hat{h}_{1,2}^* r_3 + \hat{h}_{2,2} r_4^* \\ &= \left(\left| \hat{h}_{1,1} \right|^2 + \left| \hat{h}_{2,1} \right|^2 + \left| \hat{h}_{1,2} \right|^2 + \left| \hat{h}_{2,2} \right|^2 \right. \\ &\quad \left. - \hat{h}_{1,1}^* e_{1,1} - \hat{h}_{2,1}^* e_{2,1} - \hat{h}_{1,2} e_{1,2}^* - \hat{h}_{2,2} e_{2,2}^* \right) x_1 \\ &\quad + \left(-\hat{h}_{1,1}^* e_{1,2} - \hat{h}_{2,1}^* e_{2,2} + \hat{h}_{1,2} e_{1,1}^* + \hat{h}_{2,2} e_{2,1}^* \right) x_2 \\ &\quad + \left(\hat{h}_{1,1}^* n_1 + \hat{h}_{2,1}^* n_2 + \hat{h}_{1,2} n_3^* + \hat{h}_{2,2} n_4^* \right), \end{aligned} \quad (11)$$

where terms S_α , S_β , and S_τ are the desired signal, IAI and noise, respectively. Accordingly, referring to Eq. (3) and Eq. (4), the decision metric of \tilde{x}_1 can be expressed as

$$\begin{aligned} Z_{\tilde{x}_1, i} &= \left| \sum_{\kappa=0}^{2^{SF}-1} w_{\tilde{x}_1}(\kappa T_c) \cdot \bar{w}_i^*(\kappa T_c) \right| \\ &= \begin{cases} \left| \sqrt{\frac{E_s}{2}} \left(\left| \hat{h}_{1,1} \right|^2 + \left| \hat{h}_{2,1} \right|^2 + \left| \hat{h}_{1,2} \right|^2 + \left| \hat{h}_{2,2} \right|^2 \right. \right. \\ \left. \left. - \hat{h}_{1,1}^* e_{1,1} - \hat{h}_{2,1}^* e_{2,1} - \hat{h}_{1,2} e_{1,2}^* - \hat{h}_{2,2} e_{2,2}^* \right) \right|, & i = p \\ \left| \sqrt{\frac{E_s}{2}} \left(-\hat{h}_{1,1}^* e_{1,2} + \hat{h}_{1,2} e_{1,1}^* - \hat{h}_{2,1}^* e_{2,2} \right. \right. \\ \left. \left. + \hat{h}_{2,2} e_{2,1}^* \right) + \hat{h}_{1,1}^* \phi_1 + \hat{h}_{2,1}^* \phi_2 \right|, & i \neq p, i = s_2 \\ \left| \hat{h}_{1,1}^* \phi_1 + \hat{h}_{2,1}^* \phi_2 + \hat{h}_{1,2} \phi_3^* + \hat{h}_{2,2} \phi_4^* \right|, & i \neq p, i \neq s_2 \end{cases}, \end{aligned} \quad (12)$$

where ϕ is the complex Gaussian noise process. Then, the symbol s_1 is estimated by

$$\hat{s}_1 = \arg \max_{i=0, \dots, 2^{SF}-1} (|Z_{\tilde{x}_1, i}|). \quad (13)$$

III. PERFORMANCE ANALYSIS

In this section, the average BER performance of the proposed STBC-MIMO LoRa system is analyzed. We denote $f_{Ray}(y; \sigma_y)$ and $f_{Ri}(y; m_y, \sigma_y)$ as the probability density functions (PDFs) of the Rayleigh and Rice distributions, respectively, and we denote the cumulative probability density (CDF) of Rayleigh distribution by $F_{Ray}(y; \sigma_y)$, where m_y and σ_y are the scale and location parameters of the variable y [47]. By induction on Eq. (12), we obtain the distribution of the decision metric of x_1 for an STBC-MIMO LoRa system with M transmit antennas and N receive antennas

$$Z_{\tilde{x}_1, i} \sim \begin{cases} f_{Ri} \left(\alpha; \left| \hat{\mathbf{H}} \right|_F^2 \sqrt{\frac{E_s}{rM}}, \sqrt{\frac{\left| \hat{\mathbf{H}} \right|_F^2}{2} \left(\frac{\sigma_e^2 E_s}{rM} + N_0 \right)} \right), & i = p \\ f_{Ray} \left(\beta; \sqrt{\frac{\left| \hat{\mathbf{H}} \right|_F^2}{2} \left(\frac{\sigma_e^2 E_s}{rM} + N_0 \right)} \right), & i \neq p, i = s_2, \dots, s_J \\ f_{Ray} \left(\tau; \sqrt{\frac{\left| \hat{\mathbf{H}} \right|_F^2 N_0}{2}} \right), & i \neq p, s_2, \dots, s_J \end{cases}, \quad (14)$$

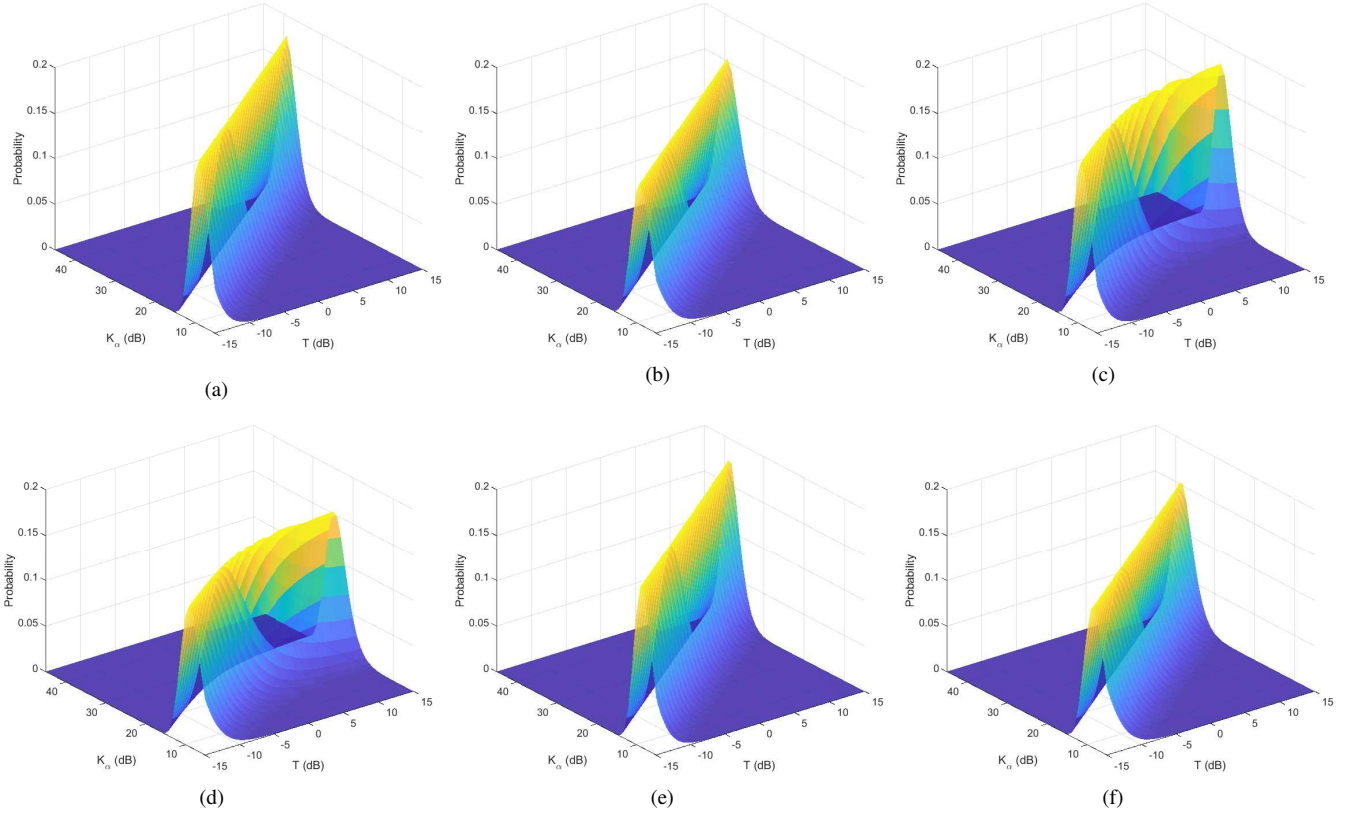


Fig. 2. The PDF of K_α versus SNR with parameters $\{r, M, N, SF, \sigma_e^2\} =$ (a) $\{1, 2, 2, 7, 0\}$, (b) $\{0.5, 3, 1, 7, 0\}$, (c) $\{1, 2, 2, 7, 0.01\}$, (d) $\{0.5, 3, 1, 7, 0.01\}$, (e) $\{1, 2, 2, 7, 1/(1 + L_p T_{eff})\}$, (f) $\{0.5, 3, 1, 7, 1/(1 + L_p T_{eff})\}$, where L_p is set to 4.

where $\|\hat{\mathbf{H}}\|_F^2 = \sum_{m=1}^M \sum_{n=1}^N |\hat{h}_{m,n}|^2$ is the square of the Frobenius norm of $\{\hat{h}_{m,n}\}$. For convenience, we denote $\|\hat{\mathbf{H}}\|_F^2$ by X . For a Rayleigh fading channel, X follows a chi-square distribution with MN degrees of freedom. Thus, the average BER of the proposed system can be expressed as

$$\begin{aligned}
 P_b &= \frac{2^{SF-1}}{2^{SF}-1} \Pr \left[\max_{i, i \neq p} (Z_{\bar{x}_1, i}) > Z_{\bar{x}_1, p} \right] \\
 &= \frac{2^{SF-1}}{2^{SF}-1} \int_0^\infty \left[1 - \Pr \left[Z_{\bar{x}_1, p|X} > \max_{i, i \neq p} (Z_{\bar{x}_1, i|X}) \right] \right] \\
 &\quad \times f_X(X) dX \\
 &= \frac{2^{SF-1}}{2^{SF}-1} \int_0^\infty \int_0^\infty \left[1 - [F_{Ray}(\alpha|X; \sigma_\beta)]^{J-1} \right. \\
 &\quad \times [F_{Ray}(\alpha|X; \sigma_\tau)]^{2^{SF}-J} \left. \times f_{Ri}(\alpha|X; m_\alpha, \sigma_\alpha) \right] \\
 &\quad \times f_X(X) d\alpha dX, \tag{15}
 \end{aligned}$$

where $f_X(X)$ is the PDF of X . To simplify Eq. (15), another equivalent form is utilized to represent P_b [18], [48], in which the error probability is expressed in terms of the noise-driven probability and the IAI-driven probability, respectively, i.e.,

$$P_b = \frac{2^{SF-1}}{2^{SF}-1} [P_{err}^N + (1 - P_{err}^N) \times P_{err}^{IAI}], \tag{16}$$

where

$$\begin{aligned}
 P_{err}^N &= \int_0^\infty \left[1 - \Pr \left[Z_{\bar{x}_1, p|X} > \max_{i, i \neq p, s_2, \dots, s_J} (Z_{\bar{x}_1, i|X}) \right] \right] \\
 &\quad \times f_X(X) dX \\
 &= \int_0^\infty \int_0^\infty \left[1 - [F_{Ray}(\alpha|X; \sigma_J)]^{2^{SF}-1} \right] \times f_{Ri}(\alpha; m_\alpha, \sigma_\alpha) \\
 &\quad \times f_X(X) d\alpha dX, \tag{17}
 \end{aligned}$$

and

$$\begin{aligned}
 P_{err}^{IAI} &= \int_0^\infty \left[1 - \Pr \left[Z_{\bar{x}_1, p|X} > \max_{i, i \neq p, i=s_2, \dots, s_J} (Z_{\bar{x}_1, i|X}) \right] \right] \\
 &\quad \times f_X(X) dX \\
 &= \int_0^\infty \int_0^\infty \left[1 - [F_{Ray}(\alpha|X; \sigma_\beta)]^{J-1} \right] \times f_{Ri}(\alpha; m_\alpha, \sigma_\alpha) \\
 &\quad \times f_X(X) dX. \tag{18}
 \end{aligned}$$

In Eqs. (17) and (18), because $f_{Ri}(\alpha|X; m_\alpha, \sigma_\alpha)$ in the integrand contains a modified Bessel function [49], the overflow and accuracy problems will be faced when the numerical calculation is performed. Considering that when the Rice factor K is large, the Rice distribution can be well approximated as a Gaussian distribution [47], thus the Rice factor K_α of $f_{Ri}(\alpha|X; m_\alpha, \sigma_\alpha)$ is further analyzed, which can be expressed as

$$K_\alpha = \frac{m_\alpha^2}{2\sigma_\alpha^2} = \frac{X \cdot T \cdot 2^{SF}}{(\sigma_e^2 \cdot T \cdot 2^{SF} + rM)}, \tag{19}$$

where $T = E_s/(N_0 \cdot 2^{SF})$ is the SNR in the LoRa communication [28]. It can be observed from Eq. (19) that since X is a random variable, K_α is also a random variable related to X . Fig. 2 shows the PDF of K_α by Monte Carlo simulation under different parameters (e.g., r , M , N , SF , T , and σ_e^2), where $\sigma_e^2 = 0$ and $\sigma_e^2 \neq 0$ correspond to the perfect CSI and the imperfect CSI scenarios, respectively, where L_p denotes the number of the pilot symbol. When σ_e^2 is nonzero and fixed, it corresponds to CEEM I, while when $\sigma_e^2 = 1/(1 + L_p T_{eff})$, it corresponds to CMME II [36], [50].⁴ It can be seen that K_α is basically distributed in the region of $K_\alpha \geq 10$ dB in both perfect CSI and imperfect CSI scenarios. Hence, the Rice distributed random variable α can approximately follow a Gaussian distribution $\mathcal{N}(m_\alpha, \sigma_\alpha^2)$ [47]. However, in the imperfect CSI scenario with CEEM I, it can be observed from Figs. 2(c) and 2(d) that K_α hardly increases with the increase of SNR in high SNR region. Therefore, considering that in presence of imperfect CSI, P_b in high SNR region is dominated by P_{err}^{IAI} , the Gaussian distribution will not be utilized to approximate the Rice distribution in the derivation of P_{err}^{IAI} in order to ensure the accuracy of the performance analysis in high SNR region (Although this phenomenon does not occur in the CEEM II, for consistency of the derivation of P_{err}^{IAI} under the CEEM I and the CEEM II, the Gaussian distribution will not be utilized to approximate the Rice distribution in the entire derivation of P_{err}^{IAI}).

In addition to the above numerical problems, $SF \in \{7, 8, \dots, 12\}$, $[F_{Ray}(\alpha|X; \sigma_J)]^{2^{SF}-1}$ in Eq. (17) has a very high complexity. Here, let $\tau_{\max} = \max_{i, i \neq p, s_2, \dots, s_J} (Z_{\bar{x}_1, i})$, and then refer to the procedure in [28] to approximate the distribution of variable τ_{\max} by a Gaussian distribution $\mathcal{N}(\mu_{\tau_{\max}}, \sigma_{\tau_{\max}}^2)$. Specifically, $\mu_{\tau_{\max}}$ and $\sigma_{\tau_{\max}}^2$ are respectively given by

$$\mu_{\tau_{\max}} = \left[X^2 \left(N_0^2 \cdot \hbar_{2^{SF}-J}^2 - \frac{N_0^2 \cdot \lambda_{2^{SF}-J}}{2} \right) \right]^{\frac{1}{4}}, \quad (20)$$

$$\sigma_{\tau_{\max}}^2 = X^2 \left(N_0 \hbar_{2^{SF}-J} - \sqrt{N_0^2 \hbar_{2^{SF}-J}^2 - \frac{N_0^2 \lambda_{2^{SF}-J}}{2}} \right), \quad (21)$$

where $\hbar_k = \sum_{q=1}^k \frac{1}{q}$ denotes the k^{th} harmonic number and $\lambda_k = \sum_{q=1}^k \frac{1}{q^2}$.

Based on the above approximation of the distribution of the random variables α and τ_{\max} , P_{err}^N can be approximated as

$$\begin{aligned} P_{err}^N &\approx \int_0^\infty Q \left(\frac{\mu_\alpha - \mu_{\tau_{\max}}}{\sqrt{\sigma_\alpha^2 + \sigma_{\tau_{\max}}^2}} \right) \cdot f_X(X) dX \\ &= \int_0^\infty Q \left(\left(\sqrt{\frac{X^2 E_s}{N_0 r M}} - \left(\hbar_{2^{SF}-J}^2 - \frac{\lambda_{2^{SF}-J}}{2} \right)^{\frac{1}{4}} \right) \right. \\ &\quad \left. \div \sqrt{\left(\frac{\sigma_e^2 E_s}{2 N_0 r M} + \frac{1}{2} \right) + \hbar_{2^{SF}-J} - \sqrt{\hbar_{2^{SF}-J}^2 - \frac{\lambda_{2^{SF}-J}}{2}}} \right) \\ &\quad \times f_X(X) dX, \end{aligned} \quad (22)$$

⁴ $T_{eff} = 2^{SF} \cdot T$ is the effective SNR for the target symbol [28].

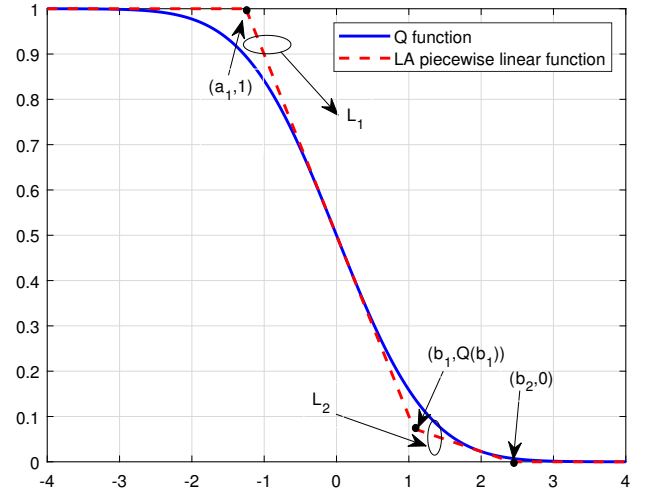


Fig. 3. Q -function and its approximated piecewise linear function.

where $Q(\cdot)$ is the Q -function [47]. Since $SF \in \{7, \dots, 12\}$, $\hbar_{2^{SF}-J} \gg \frac{\lambda_{2^{SF}-J}}{2}$. Hence, one can obtain

$$P_{err}^N \approx \int_0^\infty Q \left(\frac{A\sqrt{X} - B}{C} \right) \cdot DX^{MN-1} \cdot e^{-Ex} dX, \quad (23)$$

where $A = \sqrt{\frac{T \cdot 2^{SF}}{rM}}$, $B = \sqrt{\hbar_{2^{SF}-J}}$, $C = \sqrt{\frac{\sigma_e^2 T \cdot 2^{SF}}{2rM} + \frac{1}{2}}$, $D = \frac{1}{\Gamma(MN) \cdot (1 + \sigma_e^2)^{MN}}$, $\Gamma(\cdot)$ denotes Gamma function [51], and $E = -\frac{1}{1 + \sigma_e^2}$. Next, further derivations of P_{err}^N and P_{err}^{IAI} are performed in the perfect CSI and the imperfect CSI scenarios.

A. Perfect CSI

Since there is no IAI in the perfect CSI scenario, the BER of the proposed STBC-MIMO LoRa system only depends on the noise-driven error probability in this scenario. Since Eq. (23) has no closed-form expression, here a linear approximation (LA) approach is utilized to approximate the Q -function as a piecewise linear function (as shown in Fig. 3). Accordingly, the approximated piecewise linear function of $Q\left(\frac{A\sqrt{X}-B}{C}\right)$ can be expressed as

$$Q \left(\frac{A\sqrt{X} - B}{C} \right) \simeq \begin{cases} 1 & X \in (-\infty, a_1] \\ L_1 & X \in (a_1, b_1] \\ L_2 & X \in (b_1, b_2] \\ 0 & X \in (b_2, +\infty) \end{cases}, \quad (24)$$

where L_1 , L_2 , a_1 , b_1 , and b_2 are respectively expressed as

$$L_1 = \frac{-A^2 X}{\sqrt{8\pi} BC} + \left(\frac{B}{\sqrt{8\pi} C} + \frac{1}{2} \right), \quad (25)$$

$$L_2 = \frac{-A^2 X}{e\sqrt{8\pi} C (B + 2C)} + \frac{(B + 2C)}{e\sqrt{8\pi} C} + Q(2), \quad (26)$$

$$a_1 = \frac{2B^2 - \sqrt{8\pi} BC}{2A^2}, \quad (27)$$

$$b_1 = \left[\frac{(B + 2C) - eB}{e\sqrt{8\pi C}} + Q(2) - \frac{1}{2} \right] \times \frac{e\sqrt{8\pi BC}(B + 2C)}{A^2 [B - e(B + 2C)]}, \quad (28)$$

$$b_2 = \frac{[e\sqrt{8\pi C}(B + 2C) \times Q(2) + (B + 2C)^2]}{A^2}. \quad (29)$$

Then, the closed-form approximated average BER expression of the proposed STBC-MIMO LoRa system in the perfect CSI scenario can be obtained as

$$\begin{aligned} P_{b,pcsi} &\approx \frac{2^{\text{SF}-1}}{2^{\text{SF}} - 1} \cdot P_{err,pcsi}^{N,Appr} \\ &= \frac{2^{\text{SF}-1}}{2^{\text{SF}} - 1} \cdot D (I_1 + I_2 + I_3), \end{aligned} \quad (30)$$

Where I_1 is derived as

$$I_1 = \int_0^{a_1} 1 \cdot X^{MN-1} \cdot e^{-Ex} dX, \quad (31)$$

where $e = \sum_{k=0}^{\infty} \frac{1}{k!}$ is the base of the natural logarithm. Utilizing [51, Eq.(2.321)], I_1 can be expressed as

$$\begin{aligned} I_1 &= e^{Ea_1} \left[\sum_{k=0}^{MN-1} \frac{(-1)^k k! \binom{MN-1}{k}}{E^{k+1}} \times a_1^{(MN-1-k)} \right] \\ &- \left[\frac{(-1)^{(MN-1)} (MN-1)!}{E^{MN}} \right], \end{aligned} \quad (32)$$

Similarly, I_2 and I_3 are expressed as Eq. (33) and Eq. (34) on the next page, respectively.

B. Imperfect CSI

In the imperfect CSI scenario, LA is not utilized in the derivation due to accuracy problem.⁵ To obtain the closed-form expression for Eq. (23) in the imperfect scenario, the Gaussian-Hermite quadrature approach is utilized to evaluate P_{err}^N [52], which can be expressed as

$$\int_{-\infty}^{+\infty} f(\xi) d\xi = \sum_{\vartheta=1}^{\rho} \omega_{\vartheta} f(\xi_{\vartheta}) e^{\xi_{\vartheta}^2} + O_{\rho}, \quad (35)$$

where ρ is the number of samples and it determines the accuracy of the approximation, ξ_{ϑ} is the ϑ^{th} zero point of the Hermite polynomial, and O_{ρ} is the remaining term (when ρ approaches infinity, O_{ρ} decreases to 0), and ω_{ϑ} is the ϑ^{th} associated weight written as

$$\omega_{\vartheta} = \frac{2^{\rho} \rho! \sqrt{\pi}}{\rho^2 \Omega_{\rho-1}^2(\xi_{\vartheta})}. \quad (36)$$

To solve the integral in P_{err}^N , some mathematical processing needs to be performed first. Utilizing variable substitution $\xi = \ln(X)$, P_{err}^N can be rewritten as

$$P_{err}^N = D \int_{-\infty}^{+\infty} Q \left(\frac{A\sqrt{e^{\xi}} - B}{C} \right) \cdot e^{(MN\xi + Ee^{\xi})} d\xi, \quad (37)$$

⁵When $\sigma_e^2 \neq 0$, a_1 is less than zero in the middle and high SNR regions while the lower limit of the integral in Eq. (23) is zero. Therefore, utilizing the LA in the imperfect CSI scenario reduces the accuracy of the analysis for the error probability P_{err}^N .

$$\begin{aligned} I_2 &= \int_{a_1}^{b_1} L_2 \times X^{MN-1} e^{(EX)} dX \\ &= \frac{-A^2}{\sqrt{8\pi BC}} \left[e^{EX} \left(\sum_{k=0}^{MN} \frac{(-1)^k k! \binom{MN-1}{k}}{E^{(MN+1)}} \times X^{(MN-k)} \right) \Big|_{a_1}^{b_1} \right] + \left(\frac{B}{\sqrt{8\pi C}} + \frac{1}{2} \right) \\ &\times \left[e^{EX} \left(\sum_{k=0}^{MN-1} \frac{(-1)^k k! \binom{MN-1}{k}}{E^{MN}} X^{(MN-1-k)} \right) \Big|_{a_1}^{b_1} \right]. \end{aligned} \quad (33)$$

$$\begin{aligned} I_3 &= \int_{b_1}^{b_2} L_2 \cdot X^{MN-1} e^{Ex} dX \\ &= \frac{-A^2}{e\sqrt{8\pi C}(B + 2C)} \left[e^{EX} \left(\sum_{k=0}^{MN} \frac{(-1)^k k! \binom{MN}{k}}{E^{(MN-1)}} X^{(MN-k)} \right) \Big|_{b_1}^{b_2} \right] + \left[\frac{B + 2C}{e\sqrt{8\pi C}} + Q(2) \right] \\ &\times \left[e^{EX} \left(\sum_{k=0}^{MN-1} \frac{(-1)^k k! \binom{MN-1}{k}}{E^{MN}} X^{(MN-1-k)} \right) \Big|_{b_1}^{b_2} \right]. \end{aligned} \quad (34)$$

Therefore, by utilizing the Gaussian-Hermite approach given in Eq. (35), P_{err}^N in Eq. (23) can be approximated as

$$P_{err,icsi}^{N,Appr} = D \cdot \sum_{\vartheta=1}^{\rho} \omega_{\vartheta} Q \left(\frac{A\sqrt{e^{\xi}} - B}{C} \right) \cdot e^{(\xi_{\vartheta}^2 + MN\xi_{\vartheta} + Ee^{\xi_{\vartheta}})}, \quad (38)$$

Next, we focus on the derivation of the IAI-driven error probability as follow

$$\begin{aligned} P_{err}^{IAI} &= \int_0^{\infty} \int_0^{\infty} \left[1 - \left[1 - e^{-\frac{\alpha^2}{2\sigma_{\alpha}^2}} \right]^{J-1} \right] \\ &\times \frac{\alpha}{\sigma_{\alpha}^2} I_0 \left(\frac{m_{\alpha}\alpha}{\sigma_{\alpha}^2} \right) e^{-\frac{(\alpha^2 + m_{\alpha}^2)}{2\sigma_{\alpha}^2}} \cdot DX^{(MN-1)} \\ &\times e^{EX} d\alpha dX \\ &= D \cdot \int_0^{\infty} \int_0^{\infty} \sum_{\ell=1}^{J-1} (-1)^{\ell+1} \binom{J-1}{\ell} \cdot e^{-\frac{\ell\alpha^2}{2\sigma_{\alpha}^2}} \\ &\times \frac{\alpha}{\sigma_{\alpha}^2} I_0 \left(\frac{m_{\alpha}\alpha}{\sigma_{\alpha}^2} \right) \cdot e^{-\frac{(\alpha^2 + m_{\alpha}^2)}{2\sigma_{\alpha}^2}} \cdot X^{(MN-1)} \cdot e^{EX} d\alpha dX, \end{aligned} \quad (39)$$

where $I_0(\cdot)$ is the Bessel function of order zero and $\binom{R_1}{R_2} = \frac{R_1!}{R_2!(R_1-R_2)!}$. Owing to $\sigma_{\alpha}^2 = \sigma_{\beta}^2$, Eq. (39) becomes

$$\begin{aligned} P_{err}^{IAI} &= D \cdot \sum_{\ell=1}^{J-1} (-1)^{\ell} \binom{J-1}{\ell} \cdot e^{-\frac{\ell m_{\alpha}^2}{2(\ell+1)\sigma_{\alpha}^2}} \\ &\times \int_0^{\infty} \int_0^{\infty} \frac{\alpha}{\sigma_{\alpha}^2} I_0 \left(\frac{m_{\alpha}\alpha}{\sigma_{\alpha}^2} \right) \cdot e^{-\frac{(\ell+1)\alpha^2 + \frac{m_{\alpha}^2}{(\ell+1)}}{2\sigma_{\alpha}^2}} \\ &\times X^{(MN-1)} \cdot e^{EX} d\alpha dX, \end{aligned} \quad (40)$$

By introducing substitutions of variables $\alpha' = \frac{\alpha}{\sqrt{\ell+1}}$ and $m'_{\alpha} = m_{\alpha}\sqrt{\ell+1}$, Eq. (40) can be rewritten as [29], [47]

$$\begin{aligned} P_{err}^{IAI} &= D \cdot \sum_{\ell=1}^{J-1} (-1)^{\ell+1} \binom{J-1}{\ell} \cdot e^{-\frac{\ell m_{\alpha}^2}{2(\ell+1)\sigma_{\alpha}^2}} \\ &\times \frac{1}{\ell+1} \int_0^{\infty} \int_0^{\infty} \frac{\alpha'}{\sigma_{\alpha}^2} I_0 \left(\frac{\alpha' m'_{\alpha}}{\sigma_{\alpha}^2} \right) \cdot e^{-\frac{\alpha'^2 + m'_{\alpha}{}^2}{2\sigma_{\alpha}^2}} \\ &\times X^{(MN-1)} \cdot e^{EX} d\alpha' dX \\ &= D \cdot \sum_{\ell=1}^{J-1} \frac{(-1)^{\ell+1}}{\ell+1} \binom{J-1}{\ell} \\ &\times \int_0^{\infty} e^{-\left(\frac{\ell}{\ell+1} \cdot \frac{T \cdot 2^{SF}}{\sigma_e^2 \cdot T \cdot 2^{SF} + rM} - E \right) X} \cdot X^{(MN-1)} dX, \end{aligned} \quad (41)$$

Then, utilizing [51, Eq.(3.351)], a closed-form expression of P_{err}^{IAI} is given by

$$\begin{aligned} P_{err, clo.}^{IAI} &= D \cdot \sum_{\ell=1}^{J-1} \frac{(-1)^{\ell+1}}{\ell+1} \binom{J-1}{\ell} (MN-1)! \\ &\times \left(\frac{\ell}{\ell+1} \cdot \frac{T \cdot 2^{SF}}{\sigma_e^2 \cdot T \cdot 2^{SF} + rM} - E \right)^{-MN}. \end{aligned} \quad (42)$$

Finally, combining Eqs. (16), (38), and (42), the closed-form approximated average BER expression of the proposed STBC-MIMO LoRa system in the imperfect CSI scenario can be expressed as

$$P_{b,icsi} \approx \frac{2^{SF-1}}{2^{SF}-1} \left[P_{err,icsi}^{N,Appr} + \left(1 - P_{err,icsi}^{N,Appr} \right) \times P_{err,clo.}^{IAI} \right]. \quad (43)$$

C. Analysis of diversity order

In this subsection, for gaining more insights from the BER analysis, we investigate the asymptotic BER performance in high SNR region to analyze the diversity order of the proposed STBC-MIMO LoRa system. In the perfect CSI scenario, substituting $\sigma_e^2 = 0$ into Eq.(23), the integral-form BER expression is given by

$$\begin{aligned} P_{b,pcsi} &= \frac{2^{SF-1}}{2^{SF}-1} \cdot \frac{1}{2\Gamma(MN)} \\ &\times \int_0^{\infty} Q \left(\sqrt{\frac{T \cdot 2^{SF}}{rM}} \cdot X - B \right) \cdot X^{(MN-1)} e^{-X} dX, \end{aligned} \quad (44)$$

In high SNR region, T has a very large value, thus Eq. (44) can be approximated as

$$\begin{aligned} P_{b,pcsi,s} &\approx \frac{2^{SF-1}}{2^{SF}-1} \cdot \frac{1}{2\Gamma(MN)} \\ &\times \int_0^{\infty} Q \left(\sqrt{\frac{T \cdot 2^{SF}}{rM}} \cdot X \right) \cdot X^{(MN-1)} e^{-X} dX, \end{aligned} \quad (45)$$

where $P_{b,pcsi} \propto P_{b,pcsi,s}$. To solve the integral in Eq. (45), the following integral function can be employed [53]

$$\begin{aligned} &\int_0^{\infty} Q(\sqrt{\varpi x}) x^{\varphi-1} e^{-\frac{x}{\zeta}} dx \\ &= \frac{1}{2} \zeta^{\varphi} \Gamma(\varphi) \left[1 - \sum_{k=0}^{\varphi-1} \mu \left(\frac{1-\mu^2}{4} \right) \binom{2k}{k} \right], \end{aligned} \quad (46)$$

where $\mu = \sqrt{(\varpi\zeta)/(2+\varpi\zeta)}$. Hence, $P_{b,pcsi,s}$ in Eq. (45) can be written as

$$\begin{aligned} P_{b,pcsi,s} &= \frac{2^{SF-1}}{2^{SF}-1} \cdot \frac{1}{\Gamma(MN)} \\ &\times \frac{1}{2} \Gamma(MN) \left[1 - \sum_{k=0}^{MN-1} \mu_1 \left(\frac{1-\mu_1^2}{4} \right)^k \binom{2k}{k} \right], \end{aligned} \quad (47)$$

where $\mu_1 = \sqrt{(T \cdot 2^{SF+1})/(2rM + T \cdot 2^{SF+1})}$. According to [54], [55], Eq. (47) can be rewritten and further simplified as

$$\begin{aligned} P_{b,pcsi,s} &= \frac{2^{SF-1}}{2^{SF}-1} \cdot \frac{\Gamma(MN-1)}{\Gamma(MN)} \\ &\times \left(\frac{1-\mu_1}{2} \right)^{MN} \sum_{k=0}^{MN-1} \binom{MN-1+k}{k} \left(\frac{1+\mu_1}{2} \right)^k \\ &\approx \frac{2^{SF-1}}{2^{SF}-1} \cdot \left(\frac{rM}{2^{SF+2}} \right) \cdot \left(\frac{1}{T} \right)^{MN} \cdot \binom{2MN-1}{MN}. \end{aligned} \quad (48)$$

Hence, one can conclude from Eq. (48) that the diversity order of the proposed system in the perfect CSI scenario is MN .

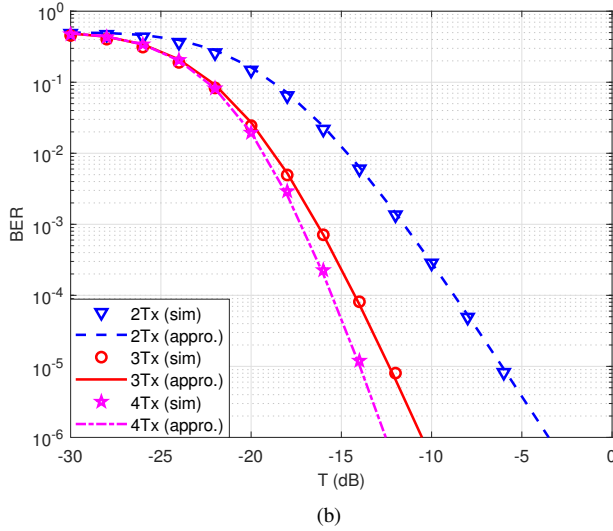
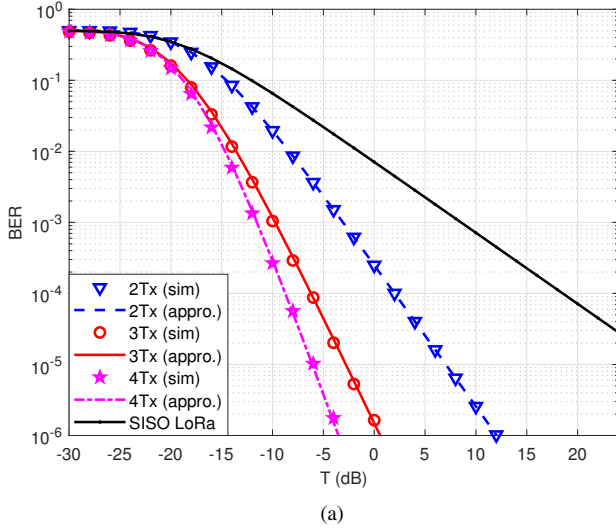


Fig. 4. Simulated and approximated BER results of the proposed STBC-MIMO LoRa system with (a) 1Rx and (b) 2Rx in the perfect CSI scenario. The simulated BER performance of the SISO LoRa system is shown with black solid line in (a).

Next, we study the diversity order of the proposed STBC-MIMO LoRa system in the imperfect CSI scenario. In this scenario, $P_{b,icsi}$ can be expressed in terms of P_{err}^N and $P_{err,cls}^{IAI}$. For the CEEM I, when T approaches to infinity, $P_{err,icsi}^N$ and $P_{err,icsi}^{IAI}$ are approximately expressed as, respectively

$$\begin{aligned}
 P_{err,icsi}^N &\approx P_{err,icsi,s}^N = \frac{1}{\Gamma(MN)(1+\sigma_e^2)^{MN}} \\
 &\times \int_0^\infty Q\left(\frac{2}{\sigma_e^2} \cdot X\right) X^{MN-1} e^{-\frac{X}{1+\sigma_e^2}} dX \\
 &= \frac{1}{2} \left[1 - \sum_{k=0}^{MN-1} \mu_2 \left(\frac{1-\mu_2^2}{4} \right) \cdot \binom{2k}{k} \right], \quad (49)
 \end{aligned}$$

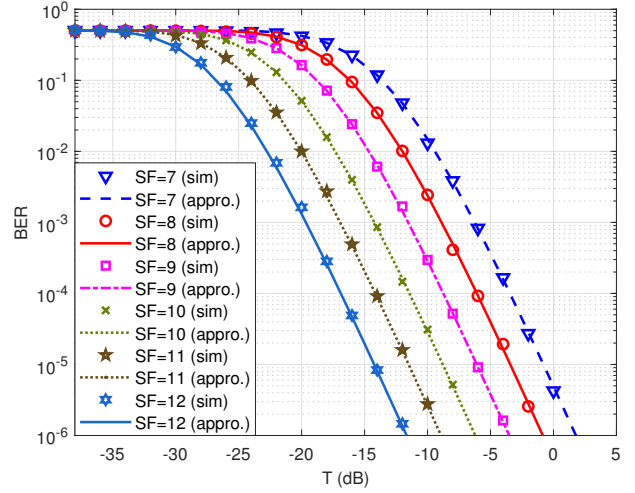


Fig. 5. Simulated and approximated BER results of the proposed STBC-MIMO LoRa system with 4Tx and 1Rx at different spreading factors in the perfect CSI scenario.

$$\begin{aligned}
 P_{err,icsi}^{IAI} &\approx P_{err,icsi,s}^{IAI} = D \cdot \sum_{\ell} \frac{(-1)^{\ell+1}}{\ell+1} \cdot \binom{J-1}{\ell} \\
 &\times (MN-1)! \times \left(\frac{\ell}{\ell+1} \cdot \frac{1}{\sigma_e^2} - E \right)^{-MN}, \quad (50)
 \end{aligned}$$

where $\mu_2 = \sqrt{(1+\sigma_e^2)/(1+2\sigma_e^2)}$. Since both $P_{err,icsi,s}^N$ and $P_{err,icsi,s}^{IAI}$ are constants, the diversity order of the proposed STBC-MIMO LoRa system is zero for CEEM I. Therefore, the error floor inevitably appear in high SNR region, and one can get the expression of error floor, given by

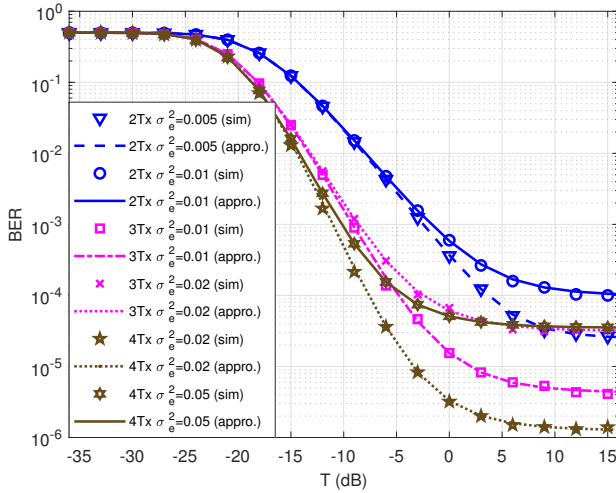
$$\begin{aligned}
 P_{err_flo} &= \frac{2^{SF-1}}{2^{SF}-1} \cdot [P_{err,icsi,s}^N + (1-P_{err,icsi,s}^N) \times P_{err,icsi,s}^{IAI}] \\
 &\approx \frac{1}{2} [P_{err,icsi,s}^N + (1-P_{err,icsi,s}^N) \times P_{err,icsi,s}^{IAI}]. \quad (51)
 \end{aligned}$$

According to Eq. (51), the error floor depends on parameters $\{M, N, \sigma_e^2\}$. For the CEEM II, as T trends to infinity, σ_e^2 becomes zero. Hence, the diversity order of the proposed system for the CEEM II is the same as that in the perfect CSI scenario, which is verified by simulations.

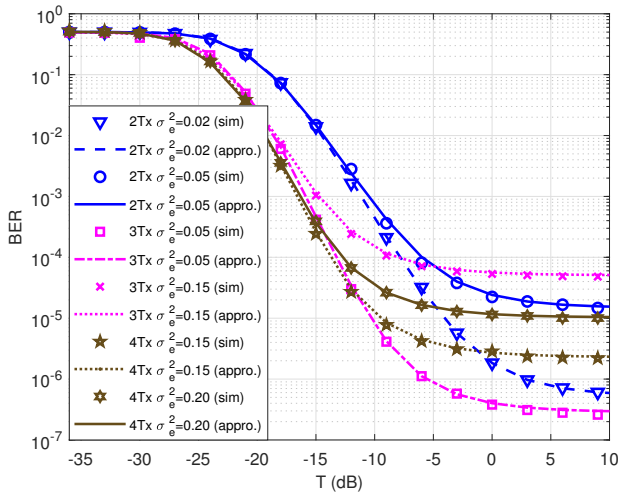
IV. SIMULATION RESULTS AND DISCUSSIONS

In this section, the performance of the proposed STBC-MIMO LoRa system with different space-time codes over a quasi-static flat Rayleigh fading channel is evaluated by simulations, and the simulation results are compared with the theoretical BER performance analysis results to verify the analysis in Sect. III. In addition, v Tx and y Rx denote v transmit antennas and y receive antennas, respectively. In the following simulations, STBCs \mathbf{G}_2 , \mathbf{G}_3 , and \mathbf{G}_4 in [46] are employed for the system with 2Tx, 3Tx, and 4Tx, respectively. Correspondingly, the code rates of 2Tx, 3Tx, and 4Tx are 1, 0.5, and 0.5, respectively.

In Fig. 4, we plot the approximated average BER curves and simulation results in the perfect CSI scenario, where SF is set to 9. From Fig. 4, the derived approximated BER results can well match with the simulated ones. Then, it can be seen



(a)



(b)

Fig. 6. Simulated and approximated BER results of the proposed STBC-MIMO LoRa system with (a)1Rx and (b)2Rx in the imperfect CSI scenario (CEEM I).

from Fig. 4(a) that utilizing the STBC-MIMO scheme can significantly improve the diversity gain of the LoRa system. From the perspective of BER performance, taking the STBC-MIMO LoRa system with 2Tx as an instance, at a BER of 10^{-4} , the proposed system has a 16-dB gain compared to the SISO system. It is observed that the STBC-MIMO LoRa system with 2Rx performs better than the system with 1Rx because the former has greater diversity order than the latter.

Fig. 5 presents the simulated and approximated BER results of the proposed STBC-MIMO LoRa system with 4Tx and 1Rx for all possible spreading factors $SF \in \{7, \dots, 12\}$ in the perfect CSI scenario. It can be seen from the figure that the simulated results are consistent with the approximated ones. In addition, BER performance increases with the increase of SF . This law in the STBC-MIMO LoRa system is consistent with that in the SISO LoRa system [18].

Furthermore, two different channel estimation error models are utilized to evaluate the proposed STBC-MIMO LoRa system with imperfect CSI, i.e., CEEM I (σ_e^2 is fixed) and

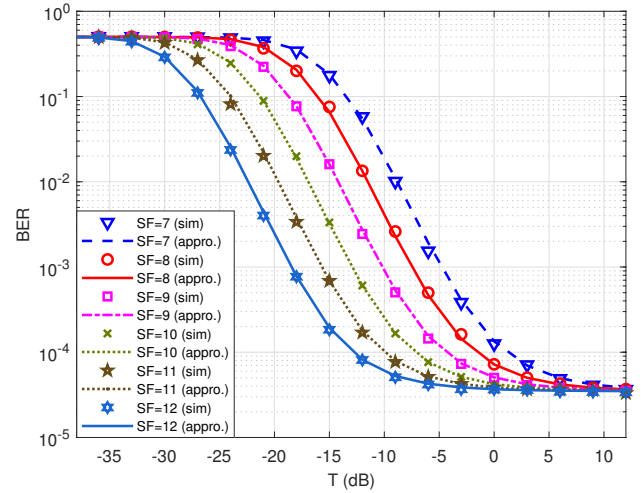


Fig. 7. Simulated and approximated BER results of the proposed STBC-MIMO LoRa system with 4Tx and 1Rx in the imperfect CSI scenario (CEEM I) at different spreading factors, where $\sigma_e^2 = 0.05$.

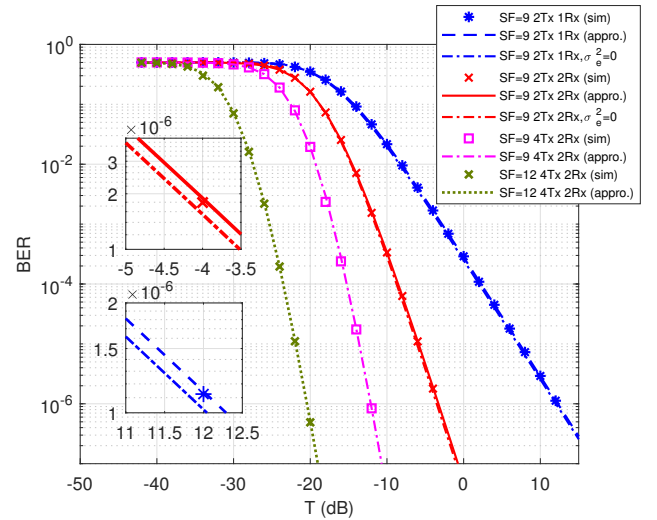


Fig. 8. Simulated and approximated BER results of the proposed STBC-MIMO LoRa system in the imperfect CSI scenario (CEEM II).

CEEM II ($\sigma_e^2 = 1/(1 + L_p T_{eff})$). L_p is set to 4. The simulated and approximated BER results of the proposed STBC-MIMO LoRa system in the imperfect CSI scenario with CEEM I are shown in Fig. 6. From this figure, it is observed that in the proposed system with the same number of the transmit and receive antenna, the error floor becomes higher as σ_e^2 increases. For a fixed σ_e^2 , increasing the number of the transmit or receive antenna can reduce the error floor.

Fig. 7 presents the simulated and approximated BER results of the proposed STBC-MIMO LoRa system with 4Tx and 1Rx at different spreading factors in the imperfect CSI scenario with CEEM I, where $SF \in \{7, \dots, 12\}$ and $\sigma_e^2 = 0.05$. As expected, for an STBC-MIMO LoRa systems with the same parameters $\{M, N, \sigma_e^2\}$, the change of SF does not affect the error floor of the BER. Then, combining Fig. 6 with Fig. 7 not only verifies the accuracy of the derived approximated BER in the imperfect CSI scenario, but also shows that the

diversity order of the proposed STBC-MIMO LoRa system is zero under the CEEM I.

Fig. 8 shows the simulated and approximated BER results of the proposed STBC-MIMO LoRa system in the imperfect CSI scenario with CEEM II (i.e., σ_e^2 is a decreasing function of SNR). It can be seen from this figure that under the CEEM II, the diversity order of the proposed system is the same as that in the perfect CSI scenario, which verifies the conclusion obtained by the analysis of the diversity order in Sect. III-C. In high SNR region, BER performance of the proposed STBC-MIMO LoRa system under CEEM II is worse than that under perfect CSI, but the system performance in these two cases is very similar because σ_e^2 is very small in high SNR region. Furthermore, the results also show that the derived approximated BER expression is valid for CEEM II.

V. CONCLUSIONS

In this paper, an STBC-MIMO LoRa system has been presented and its theoretical performance has been carefully studied. To be specific, the closed-form approximated BER expression of the proposed STBC-MIMO LoRa system for the perfect and imperfect CSI scenarios has been derived. As a further advance, the diversity order of the proposed system has been analyzed. According to the analyzed results, the diversity order of the proposed system is zero in the imperfect CSI scenario with CEEM I, hence the error floor appears in high SNR region. In addition, full-diversity order $d = MN$ can be achieved in the imperfect CSI scenario with CEEM II and the perfect CSI scenario. Simulated results not only are in well agreement with the theoretical ones, but also verify the excellent performance and potential of the proposed STBC-MIMO LoRa system.

REFERENCES

- [1] M. R. Palattella, M. Dohler, A. Grieco, G. Rizzo, J. Torsner, T. Engel, and L. Ladid, "Internet of things in the 5G era: enablers, architecture, and business models," *IEEE J. Sel. Areas Commun.*, vol. 34, no. 3, pp. 510–527, Mar. 2016.
- [2] C. Bernier, F. Dehmas, and N. Deparis, "Low complexity LoRa frame synchronization for ultra-low power software-defined radios," *IEEE Trans. Commun.*, pp. 1–1, Feb. 2020.
- [3] A. Hoglund, X. Lin, O. Liberg, A. Behravan, E. A. Yavuz, M. Van Der Zee, Y. Sui, T. Tirronen, A. Ratilainen, and D. Eriksson, "Overview of 3GPP release 14 enhanced NB-IoT," *IEEE Netw.*, vol. 31, no. 6, pp. 16–22, Nov./Dec. 2017.
- [4] M. Lauridsen, B. Vejlgard, I. Z. Kovacs, H. Nguyen, and P. Mogensen, "Interference Measurements in the European 868 MHz ISM band with focus on LoRa and SigFox," in *2017 IEEE Wireless Communications and Networking Conference (WCNC)*, Mar. 2017, pp. 1–6.
- [5] J. Lim and Y. Han, "Spreading factor allocation for massive connectivity in LoRa systems," *IEEE Commun. Lett.*, vol. 22, no. 4, pp. 800–803, Apr. 2018.
- [6] U. Raza, P. Kulkarni, and M. Sooriyabandara, "Low power wide area networks: An overview," *IEEE Commun. Surveys Tut.*, vol. 19, no. 2, pp. 855–873, secondquarter. 2017.
- [7] D. Croce, M. Gucciardo, S. Mangione, G. Santaromita, and I. Tinnirello, "LoRa technology demystified: from link behavior to cell-level performance," *IEEE Trans. Wireless Commun.*, vol. 19, no. 2, pp. 822–834, Feb. 2020.
- [8] L. Vangelista, "Frequency shift chirp modulation: the LoRa modulation," *IEEE Signal Process. Lett.*, vol. 24, no. 12, pp. 1818–1821, Feb. 2017.
- [9] T. Elshabrawy and J. Robert, "Capacity planning of LoRa networks with joint noise-limited and interference-limited coverage considerations," *IEEE Sensors J.*, vol. 19, no. 11, pp. 4340–4348, June. 2019.
- [10] S. Wang, Y. Chen, T. Chen, C. Chang, Y. Cheng, C. Hsu, and Y. Lin, "Performance of LoRa-based IoT applications on campus," in *2017 IEEE 86th Vehicular Technology Conference (VTC-Fall)*, Sept. 2017, pp. 1–6.
- [11] O. Georgiou and U. Raza, "Low power wide area network analysis: can LoRa scale?" *IEEE Wireless Commun. Lett.*, vol. 6, no. 2, pp. 162–165, Apr. 2017.
- [12] K. E. Nolan, W. Guibene, and M. Y. Kelly, "An evaluation of low power wide area network technologies for the Internet of Things," in *2016 International Wireless Communications and Mobile Computing Conference (IWCMC)*, Sept. 2016, pp. 439–444.
- [13] J. Petajajarvi, K. Mikhaylov, A. Roivainen, T. Hanninen, and M. Pettissalo, "On the coverage of LPWANs: range evaluation and channel attenuation model for LoRa technology," in *2015 14th International Conference on ITS Telecommunications (ITST)*, Dec. 2015, pp. 55–59.
- [14] D. Bankov, E. Khorov, and A. Lyakhov, "Mathematical model of LoRaWAN channel access," in *2017 IEEE 18th International Symposium on A World of Wireless, Mobile and Multimedia Networks (WoWMoM)*, June. 2017, pp. 1–3.
- [15] F. Van den Abeele, J. Haxhibeqiri, I. Moerman, and J. Hoebeke, "Scalability analysis of large-scale LoRaWAN networks in ns-3," *IEEE Internet of Things Journal*, vol. 4, no. 6, pp. 2186–2198, Dec. 2017.
- [16] A. Augustin, J. Yi, C. Thomas, and T. William, "A study of LoRa: long range & low power networks for the Internet of Things," *Sensors*, vol. 16, no. 9, pp. 1466–1483, Sept. 2016.
- [17] K. Mikhaylov, J. Petajajarvi, and T. Haenninen, "Analysis of capacity and scalability of the LoRa low power wide area network technology," in *European Wireless 2016; 22th European Wireless Conference*, Dec. 2016, pp. 1–6.
- [18] O. Afisiadis, M. Cotting, A. Burg, and A. Balatsoukas-Stimming, "On the error rate of the LoRa modulation with Interference," *IEEE Trans. Wireless Commun.*, vol. 19, no. 2, pp. 1292–1304, Feb. 2020.
- [19] R. Fernandes, R. Oliveira, M. Lufs, and S. Sargento, "On the real capacity of LoRa networks: the impact of non-destructive communications," *IEEE Commun. Lett.*, vol. 23, no. 12, pp. 2437–2441, Dec. 2019.
- [20] C. Liao, G. Zhu, D. Kuwabara, M. Suzuki, and H. Morikawa, "Multi-hop LoRa networks enabled by concurrent transmission," *IEEE Access*, vol. 5, pp. 21 430–21 446, 2017.
- [21] G. Zhu, C. Liao, T. Sakdejayont, I. Lai, Y. Narusue, and H. Morikawa, "Improving the capacity of a mesh LoRa network by spreading-factor-based network Clustering," *IEEE Access*, vol. 7, pp. 21 584–21 596, 2019.
- [22] P. Branch and T. Cricenti, "A LoRa based wireless relay network for actuator data," in *2020 International Conference on Information Networking (ICOIN)*, Jan. 2020, pp. 190–195.
- [23] S. S. Borkotoky, U. Schilcher, and C. Bettstetter, "Cooperative relaying in LoRa sensor networks," in *2019 IEEE Global Communications Conference (GLOBECOM)*, Dec. 2019, pp. 1–5.
- [24] O. B. Seller and N. Sornin, "Low power long range transmitter," U.S. Patent 47 720 329, Aug. 7, 2014.
- [25] M. Knight and B. Seeber, "Decoding LoRa: realizing a modern LPWAN with SDR," in *Proceedings of the GNU Radio Conference*, vol. 1, no. 1, Sept. 2016.
- [26] R. Pieter, Q. Peter, L. Wim, and T. William, "A multi-channel software decoder for the LoRa modulation scheme," in *International Conference on Internet of Things, Big Data and Security (IoTBDs)*, Mar. 2018, pp. 41–51.
- [27] M. Chiani and A. Elzanaty, "On the LoRa modulation for IoT: waveform properties and spectral analysis," *IEEE Internet Things J.*, vol. 6, no. 5, pp. 8463–8470, Oct. 2019.
- [28] T. Elshabrawy and J. Robert, "Closed-form approximation of LoRa modulation BER performance," *IEEE Commun. Lett.*, vol. 22, no. 9, pp. 1778–1781, Sept. 2018.
- [29] C. Ferreira Dias, E. Rodrigues de Lima, and G. Fraidenraich, "Bit error rate closed-form expressions for LoRa systems under nakagami and rice fading channels," *Sensors*, vol. 19, no. 20, p. 4412, Oct. 2019.
- [30] R. Bomfin, M. Chafii, and G. Fettweis, "A novel modulation for IoT: PSK-LoRa," in *2019 IEEE 89th Vehicular Technology Conference (VTC2019-Spring)*, Mar. 2019, pp. 1–5.
- [31] T. Elshabrawy and J. Robert, "Interleaved chirp spreading LoRa-based modulation," *IEEE Internet Things J.*, vol. 6, no. 2, pp. 3855–3863, Apr. 2019.
- [32] L. Vangelista and A. Cattapan, "A new LoRa-compatible modulation improving the LoRaWAN network level performance," in *2019 IEEE Latin-American Conference on Communications (LATINCOM)*, Nov. 2019, pp. 1–6.

- [33] J. Xu, P. Zhang, S. Zhong, and L. Huang, "Discrete particle swarm optimization based antenna selection for MIMO LoRa IoT systems," in *2019 Computing, Communications and IoT Applications (ComComAp)*, Oct. 2019, pp. 204–209.
- [34] F. Wunsch, D. Weber, H. Jakel, and F. K. Jondral, "Experimental evaluation of the long-range MIMO outdoor channel at 2.4 GHz," in *2019 IEEE 89th Vehicular Technology Conference (VTC2019-Spring)*, May. 2019, pp. 1–5.
- [35] A. I. Petrariu, A. Lavric, and E. Coca, "VLC for vehicular communications: A multiple input multiple output (MIMO) approach," in *2018 International Conference on Development and Application Systems (DAS)*, May. 2018, pp. 134–137.
- [36] X. Yu, W. Xu, S. Leung, and J. Wang, "Unified performance analysis of transmit antenna selection with OSTBC and imperfect CSI over nakagami- m fading channels," *IEEE Trans. Veh. Technol.*, vol. 67, no. 1, pp. 494–508, Jan. 2018.
- [37] J. R. Magnus and H. Neudecker, *Matrix Differential Calculus with Applications in Statistics and Econometrics*. Wiley, 1988.
- [38] H. X. Nguyen, H. H. Nguyen, and T. Le-Ngoc, "Amplify-and-forward relaying with M-FSK modulation and coherent detection," *IEEE Trans. Commun.*, vol. 60, no. 6, pp. 1555–1562, June. 2012.
- [39] V. Berg, J. Dore, and V. Mannoni, "Channel estimation strategy for LPWA Transmission at low SNR: application to turbo-FSK," in *2019 IEEE 89th Vehicular Technology Conference (VTC2019-Spring)*, May. 2019, pp. 1–5.
- [40] V. Tarokh, H. Jafarkhani, and A. R. Calderbank, "Space-time block codes from orthogonal designs," *IEEE Trans. Inf. Theory*, vol. 45, no. 5, pp. 1456–1467, July. 1999.
- [41] Hyundong Shin and Jae Hong Lee, "Performance analysis of space-time block codes over keyhole nakagami- m fading channels," *IEEE Trans. Veh. Technol.*, vol. 53, no. 2, pp. 351–362, Mar. 2004.
- [42] X. Yu, X. Yin, S. H. Leung, and Y. Rui, "Precoding scheme for space-time-coded multipleinput-multiple-output system with estimation error and feedback delay in Rayleigh fading channel," *IET Commun.*, vol. 6, no. 16, pp. 2525–2533, Nov. 2012.
- [43] Q. Li, M. Wen, E. Basar, H. V. Poor, B. Zheng, and F. Chen, "Diversity enhancing multiple-mode OFDM with index modulation," *IEEE Trans. Commun.*, vol. 66, no. 8, pp. 3653–3666, Aug. 2018.
- [44] P. Aquilina and T. Ratnarajah, "Linear interference alignment in full-duplex MIMO networks with imperfect CSI," *IEEE Trans. Commun.*, vol. 65, no. 12, pp. 5226–5243, Dec. 2017.
- [45] A. E. Canbilen, S. S. Ikki, E. Basar, S. S. Gultekin, and I. Develi, "Joint impact of I/Q imbalance and imperfect CSI on SM-MIMO systems over Generalized Beckmann Fading Channels: Optimal Detection and Cramer-Rao Bound," *IEEE Trans. Wireless Commun.*, pp. 1–1, 2020.
- [46] V. Tarokh, H. Jafarkhani, and A. R. Calderbank, "Space-time block coding for wireless communications: performance results," *IEEE J. Sel. Areas Commun.*, vol. 17, no. 3, pp. 451–460, Mar. 1999.
- [47] J. G. Proakis and M. Salehi, *Digital Communications*. New York, NY, USA: McGraw-Hill, 2007.
- [48] T. Elshabrawy and J. Robert, "Analysis of BER and coverage performance of LoRa modulation under same spreading factor interference," in *2018 IEEE 29th Annual International Symposium on Personal, Indoor and Mobile Radio Communications (PIMRC)*, Sept. 2018, pp. 1–6.
- [49] G. N. Watson, *A Treatise on the Theory of Bessel Functions*. London, UK: Cambridge University Press, 1952.
- [50] W. M. Gifford, M. Z. Win, and M. Chiani, "Diversity with practical channel estimation," *IEEE Trans. Wireless Commun.*, vol. 4, no. 4, pp. 1935–1947, Jul. 2005.
- [51] I. S. Gradshteyn and I. M. Ryzhik, *Table of integrals, series and products*, 7th ed. Berkeley, CA, USA: Academic Press, 2007.
- [52] M. Abramowitz and I. A. Stegun, *Handbook of Mathematical Functions: With Formulas, Graphs, and Mathematical Tables*. New York, USA: Dover, 1996.
- [53] G. L. Stüber, *Principles of Mobile Communication*, 1st ed. USA: Kluwer Academic Publishers, 1996.
- [54] G. Kaddoum, H. Tran, L. Kong, and M. Atallah, "Design of simultaneous wireless information and power transfer scheme for short reference DCSK communication systems," *IEEE Trans. Commun.*, vol. 65, no. 1, pp. 431–443, Jan. 2017.
- [55] G. Cai, Y. Fang, G. Han, J. Xu, and G. Chen, "Design and analysis of relay-selection strategies for two-way relay network-coded DCSK Systems," *IEEE Trans. Veh. Technol.*, vol. 67, no. 2, pp. 1258–1271, Feb. 2018.